JGR Atmospheres

RESEARCH ARTICLE
10.1029/2019JD030391

Atmospheric Photolysis of Methyl Ethyl, Diethyl, and Propyl Ethyl Ketones: Temperature-Dependent UV Absorption Cross Sections

Jared F. Brewer[1], Dimitrios K. Papanastasiou[2,3], James B. Burkholder[2], Emily V. Fischer[1], Yangang Ren[4], Abdelwahid Mellouki[4], and A. R. Ravishankara[1,5]

[1]Department of Atmospheric Science, Colorado State University, Fort Collins, CO, USA, [2]Earth System Research Laboratory, Chemical Sciences Division, National Oceanic and Atmospheric Administration, Boulder, CO, USA, [3]Cooperative Institute for Research in Environmental Sciences, University of Colorado Boulder, Boulder, CO, USA, [4]Institut de Combustion, Aérothermique, Réactivité et Environnement (ICARE), Orleans, France, [5]Department of Chemistry, Colorado State University, Fort Collins, CO, USA

Key Points:
- We report UV absorption spectra of methyl ethyl (MEK) and diethyl ketone (DEK) at 242-320 K and that of propyl ethyl ketone (PEK) at 296 K
- Including the temperature dependence of absorption reduces the photolysis rate of these species in the upper troposphere by ~25%
- We present a physical model representing of the temperature dependence of these spectra, suitable for inclusion in atmospheric models

Supporting Information:
- Supporting Information S1
- Table S1
- Table S2
- Table S3
- Table S4
- Data S1
- Data S2

Correspondence to:
J. F. Brewer, E. V. Fischer, and A. R. Ravishankara,
jared.brewer@colostate.edu;
a.r.ravishankara@colostate.edu;
evf@rams.colostate.edu

Citation:
Brewer, J. F., Papanastasiou, D. K., Burkholder, J. B., Fischer, E. V., Ren, Y., Mellouki, A., & Ravishankara, A. R. (2019). Atmospheric photolysis of methyl ethyl, diethyl, and propyl ethyl ketones: Temperature-dependent UV absorption cross sections. *Journal of Geophysical Research: Atmospheres*, *124*, 5906–5918. https://doi.org/10.1029/2019JD030391

Received 31 JAN 2019
Accepted 21 APR 2019
Accepted article online 2 MAY 2019
Published online 4 JUN 2019

Author Contributions:
Conceptualization: Jared F. Brewer, James B. Burkholder
Data curation: Jared F. Brewer
Formal analysis: Jared F. Brewer, Dimitrios K. Papanastasiou
Funding acquisition: James B. Burkholder
(continued)

Abstract Ketone photolysis is a potentially important source of HO_x radicals in the upper troposphere. To represent this photolysis, models need to include actinic flux, quantum yield, and absorption cross sections over a range of atmospherically relevant conditions. This work seeks to improve the representation of ketone ultraviolet (UV) absorption by quantifying it as a function of temperature. We present observations of 1-nm resolution absorption cross sections from 200 to 335 nm of methyl ethyl ketone (MEK) and diethyl ketone (DEK) at temperatures between 242 and 320 K, as well as propyl ethyl ketone (PEK) cross sections at 296 K. Our measured room temperature absorption cross sections agree to within 2%, 2%, and 5% with previous studies for MEK, DEK, and PEK spectra, respectively. We parameterize the temperature dependence of the cross sections of MEK and DEK using a two-state model, which reproduces our experimental results well. With additional assumptions, this model can be applied to the temperature dependence of PEK in the absence of experimental data. This model is appropriate for atmospherically relevant temperatures both inside and outside the temperatures used in this study and is suitable for incorporation into model atmospheric photolysis schemes. R programs to facilitate usage of these data are included in the supporting information. Inclusion of temperature-dependent absorption cross sections in atmospheric photolysis calculations decreased the rate coefficients of MEK, DEK, and PEK photolysis in the upper troposphere when compared to those calculated using only the room temperature cross sections; the decrease can be as large as 20–25%.

1. Introduction

The primary HO_x ($OH + HO_2$) source in the global troposphere is believed to be the photolysis of ozone (O_3) to produce $O(^1D)$, whose subsequent reaction with water vapor produces OH radicals. Ketones are an important family of atmospheric trace gases with potential to serve as an additional and significant source of HO_x radicals in the upper troposphere (McKeen et al., 1997; Singh et al., 1995; Wennberg et al., 1998). Recent work suggests that the magnitude of the HO_x source from acetone photolysis in the upper troposphere, where water vapor concentrations are small, could be as much as that via O_3 photolysis (Neumaier et al., 2014).

Methyl ethyl ketone (MEK, 2-butanone), the next most emitted/produced ketone, is understudied relative to acetone. Ambient measurements in the troposphere suggest that MEK mixing ratios are approximately one quarter of those of acetone (Moore et al., 2012; Singh et al., 2004). MEK atmospheric lifetime against oxidation by OH is slightly shorter than that of acetone: ~5–13 days for MEK (Grant et al., 2008; Romero et al., 2005) as compared to ~19 days for acetone (Brewer et al., 2017). In contrast to acetone and MEK, diethyl ketone (DEK, 3-pentanone) and propyl ethyl ketone (PEK, 3-hexanone) have hardly been investigated, and we are unaware of reports of atmospheric concentrations of these compounds. However, DEK and PEK can be directly emitted into the atmosphere or secondarily produced by the oxidation of alkanes and alcohols (Siegel & Eggerdorfer, 1985; Singh et al., 2004; Yañez-Serrano et al., 2016). The ultraviolet (UV) absorption cross section of DEK and PEK in the actinic region are similar to that of MEK (Horowitz, 1999; Keller-Rudek et al., 2013; Martinez et al., 1992), and the rate coefficient for DEK's reaction with OH

Investigation: Jared F. Brewer, Dimitrios K. Papanastasiou, James B. Burkholder, Yangang Ren, Abdelwahid Mellouki
Methodology: Jared F. Brewer, Dimitrios K. Papanastasiou, James B. Burkholder, Abdelwahid Mellouki
Resources: Jared F. Brewer, Dimitrios K. Papanastasiou, James B. Burkholder, Yangang Ren, Abdelwahid Mellouki
Software: Jared F. Brewer
Validation: Jared F. Brewer
Visualization: Jared F. Brewer
Writing - original draft: Jared F. Brewer
Writing – review & editing: Jared F. Brewer, Dimitrios K. Papanastasiou, James B. Burkholder, Yangang Ren, Abdelwahid Mellouki

radicals is approximately 2.5 times larger than that of MEK (Calvert et al., 2011). By analogy to acetone and MEK, DEK and PEK could potentially contribute to production of HO_x and acyl peroxy nitrates in the troposphere.

Characterization of ketone photolysis pathways is needed because it produces HO_x. Ketones are photolyzed in the troposphere between ~290 and 350 nm. Absorption in this range is due to an electronic transition centered around the CO bond, which is the chromophore. Following excitation to the singlet upper state, the molecule quickly undergoes intersystem crossing to a longer-lived triplet state, from which it can dissociate or be quenched (Haas, 2003). Radiative deactivation can be shown to be essentially negligible at tropospheric pressures given the rapid intersystem crossing to the triplet state and long radiative lifetime of the triplet state (Haas, 2003). The exact amount of HO_x produced from the photolysis of ketones depends on the abundance of NO_x, possibility of wet scavenging, and transport to other regions.

Keller-Rudek et al. (2013) have summarized all the available cross sections data on ketones. Multiple measurements of the absorption cross sections of MEK (Martinez et al., 1992; McMillan, 1966; Yujing & Mellouki, 2000) and DEK (Koch et al., 2008; Koch & Hanson, 2003; McMillan, 1966) exist at room temperature and higher. PEK cross sections have been reported at only room temperature. (Horowitz, 1999). Nádasdi et al. (2007) have reported MEK cross sections at atmospherically relevant lower temperatures but only at a few select wavelengths. Therefore, measurements of the absorption spectra of MEK and DEK at lower atmospheric temperatures are needed to accurately represent their photolysis in chemical transport models and to calculate their HO_x production potential in the troposphere, especially at the upper troposphere where the temperatures are lower than 298 K.

In this paper, we report absorption cross sections of MEK and DEK (along with their uncertainties) between 200 and 335 nm at temperatures ranging from 242 to 320 K, with a spectral resolution of 1 nm. We also report absorption cross sections for PEK at the same resolution and wavelengths at 296 K. The measured temperature-dependent cross sections are parameterized for use in models. The data are also used to calculate representative first-order rate coefficients for the photodissociation (J values) of each compound for a few representative sets of atmospheric conditions. The model calculations enable us to contextualize the atmospheric importance of the cross section temperature dependence to the photolysis rate of these compounds, as well as provide atmospheric modelers a basis for comparison to their own ketone photolysis rate calculations.

2. Materials and Methods

2.1. Experimental Setup

A schematic of the system used to measure the gas phase spectra of MEK, DEK, and PEK is shown in Figure 1. This apparatus is similar to those used in past studies for similar measurements (e.g., Papanastasiou et al., 2011). Two absorption cells, one at room temperature and another at temperature of interest, were connected in series. The same mixture of a given ketone in a diluent gas was flowed through each absorption cell; in some instances, the measurements were made using static mixtures, which filled both cells.

The absorption spectra of MEK, DEK, and PEK were measured between 200 and 335 nm and at the different temperatures using the apparatus shown in Figure 1. This setup consisted of UV/visible light from a collimated 30-W D_2 lamp, a temperature-regulated absorption cell, an absorption cell maintained at room temperature, and a 0.5-m spectrometer equipped with a charge-coupled device (CCD) detector. The absorption cell (shown in Figure 1 and labeled D2/CCD cell) was a jacketed Pyrex tube (I.D. ~2.5 cm) where the temperature-controlled section was 90.5 cm long. The inset quartz windows ensured that the entire absorption path length was at the specified temperature. This cell was cooled or heated by flowing a silicone fluid from a temperature-controlled bath. The temperature was constant to within 2 K over the entire length of the tube for all temperatures except at the lowest temperature of the study where the difference between the coolant entrance and exits ports was ~5 K. The temperature in the cell was taken to be the average of the temperature between the two ends. The measured temperatures were accurate to 0.5 K. The output of the D_2 lamp was collimated, passed through the absorption cell, and focused onto the entrance slit of the 0.5-m spectrometer which was equipped with a 512 × 2,048-pixel CCD camera. Only the central (~100

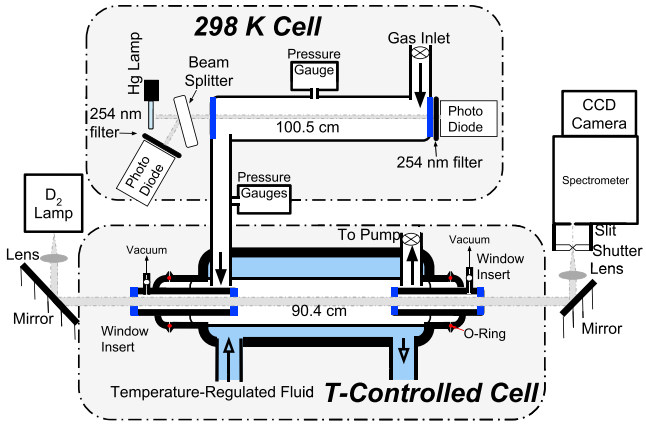

Figure 1. A schematic of the ultraviolet/visible absorption apparatus, which consists of two cells, one temperature controlled and illuminated with deuterium lamp (D_2/CCD cell) and one at room temperature illuminated by a mercury lamp (Hg/PD cell). Pressure is measured using 100- and 1,000-torr capacitance manometers. CCD = charge-coupled device.

× 2,048 array) pixels were used. The entrance slit width was adjusted to 100 μm that yielded a resolution of ~1 nm as measured by the width of a mercury atomic line. A mechanical shutter in front of the entrance slit controlled the exposure (roughly 0.3 s) such that the CCD pixels were almost completely filled (~80–90%) when the absorption cell was empty. The absorbance at each pixel was calculated using the linearized Beer-Lambert law:

$$A(\lambda) = -\ln\left(\frac{I_0(\lambda)}{I(\lambda)}\right) = \sigma(\lambda, T)\times[\text{sample}]\times L \quad (1)$$

where $I_0(\lambda)$ and $I(\lambda)$ were the intensities measured at each wavelength with the cell either empty or filled with the nonabsorbing diluent gas and with the absorbant in the cell, respectively. $\sigma(\lambda,T)$ was the ketone cross section at wavelength λ and at the temperature of the cell, [sample] was the ketone concertation in the absorption cell, and L was the absorption path length. Typically, 120 spectra were measured and coadded to obtain each $I(\lambda)$ and $I_0(\lambda)$. The measured absorbance at each wavelength varied linearly with ketone concentration. The absorption spectrum reported in this work was measured at the highest concentration practicable for the temperature and species in question, that is, our best quality spectrum with the highest possible absorbance (<1.1, base e absorbance) and lowest possible baseline fluctuation (<0.001 absorbance unit). The entire absorption spectrum was then converted to cross sections by scaling to the cross section at the peak of the near UV band (~280 nm) measured following a Beer's law analysis. Ketone concentration in the absorption cells was calculated using pressure measurements and the mixing ratio of manometrically prepared ketone/N_2 mixtures in 12-L Pyrex bulbs.

A second cell, held at room temperature, was used to measure the ketone absorbance at 254 nm. This cell (Hg/PD cell) was 100.4 cm long with quartz windows. UV light from a pen-ray mercury lamp (254-nm Hg line) was passed through this cell to measure the absorbance at room temperature at this one fixed wavelength. Both the input and transmitted 254-nm light intensities were measured using two photodiodes, positioned before and after the UV beam passed through the cell (Figure 1). This arrangement enabled precise measurements of the attenuation by continually accounting for the lamp intensity fluctuation. Absorbance was calculated using the Beer-Lambert law as in the D2/CCD cell (equation (1)). In the Hg/PD cell, however, $I_0(\lambda)$ and $I(\lambda)$ represented the ratios between the intensities measured by the photodiode at the far end of the cell (normalized to the measured lamp input) with and without a sample present. Absorbances over a range of concentrations were measured and plotted against the concentration calculated using manometric measurements and sample mixing ratio in the mixture of ketone in bath gas. The absorption cross section (σ_{254}) at 254 nm was calculated using linear unweighted least squares regression. Once the absorption cross section at 254 nm was established, the ketone concentration in the temperature variable could be derived from the room temperature 254-nm measurements.

The absorption cells were flushed with bath gas (He, ultrahigh purity, >99.99%) and then evacuated to measure $I_0(\lambda)$ prior to filling or flowing through them with ketones at known concentrations. Subsequent to the measurements with the ketone to obtain $I(\lambda)$, the cell was again evacuated or filled with the bath gas to obtain another value of $I_0(\lambda)$. Comparing the $I_0(\lambda)$ measured before and after filling with the ketone mixture allowed us to verify that the lamps and optical systems were stable during the measurement of $I(\lambda)$. These measurements also helped ascertain if ketones were sticking on the surfaces or the absorption cell and cold windows. We recorded six ketone spectra at each temperature with different concentrations in the cell. The system was plumbed such that sample flowed first into the Hg/PD cell, then to the D2/CCD cell; however, we repeated several of the individual experiments with the flow reversed, and the results were not different; that is, ketone was not lost in the cells. The measured absorbance at 254 nm at 298 K in the Hg/PD cell agreed to within 1% with that in the D2/CCD cell.

A large range of ketones concentrations were used in determining the cross sections of MEK. However, the vapor pressures of DEK at 253 and 242 K are 1.29 and 0.43 torr, respectively (Collerson et al., 1965; Majer

et al., 1985) and that of PEK is ~3 torr at 273 K (Collerson et al., 1965; Majer et al., 1985). Therefore, we were constrained to measuring DEK cross sections to $T > 242$ K and PEK cross sections to only 298 K.

2.2. Materials and Handling

MEK, DEK, and PEK samples were purchased from Sigma Aldrich and had stated chemical purities of ≥99.7%, ≥99%, and ≥99%, respectively. The liquids were degassed by freeze-pump-thaw cycles prior to use. The samples were vaporized into the 12-L glass bulbs and diluted with N_2 (ultrahigh purity, >99.99%, Matheson Tri-Gas company) to a total pressure of ~800 torr; the mixing ratios of ketones in N_2 ranged between 1% and 3%. The mixing ratio of ketones in these mixtures was also measured using a multipass infrared (IR) absorption cell with a total optical path length of 485 cm using the IR cross section from Sharpe et al. (2004). The mixing ratios derived from IR and manometric measurements agreed to within ~2–3%. We further verified that the composition of the mixture did not change over time by repeatedly measuring the IR absorption over the course of several weeks of the measurements.

3. Results

3.1. Measured Absorption Cross Sections

The top and middle panels of Figure 2 show the absorption cross sections of MEK and DEK at five temperatures. The lower panel shows the absorption cross sections of PEK at room temperature. These cross sections are also tabulated in the supporting information (Table S1). The ketones have large absorption cross sections at ~200 nm corresponding to the $\pi \rightarrow \pi^*$ electronic transition. These wavelengths, however, are less important for tropospheric photolysis since the actinic flux at wavelengths less than 280 nm is negligible in this region. All three species exhibit a minimum in cross sections around ~210 nm. The peak of the $n \rightarrow \pi^*$ electronic transition is around 277 nm. The absorption due to the $n \rightarrow \pi^*$ transition between ~280 and 335 nm is most relevant for tropospheric photolysis.

Figure 3 shows the ratios of absorption cross sections at various temperatures, $\sigma(T)$, to those measured at 298 K, σ(298 K), for both MEK and DEK. The UV absorption of MEK and DEK increases with increasing temperature at wavelengths ≥277 nm. As temperature increases, the absorption band broadens and the cross sections at longer wavelengths increase. Temperature dependence of the cross sections for MEK and DEK differ at short wavelengths, <240 nm. The key point to note is that the cross sections have simpler relationships with temperature within the atmospherically relevant wavelength region.

We have also plotted the fractional uncertainties in the measured cross sections at each wavelength in the supporting information (Figure S1). We report cross sections at wavelengths where absorbances were at least 0.015–0.02, 10 times our detection limit of 0.0015–0.002 at the 3σ level. The reported uncertainty in the UV cross sections of MEK, DEK, and PEK is at the 2σ level and includes (i) the precision of the cross section at its peak (~1%); (ii) the fluctuation of the D_2 light intensity (baseline stability) which is typically ~0.1% at wavelengths longer than 215 nm; (iii) the accuracy of the pressure measurements (~0.5%) for the mixture preparation as well as for pressure measurement in the absorption cells; and (iv) the uncertainty in the optical path length (~0.2 cm) Because these factors are assumed to be uncorrelated, the total uncertainty in the measured absorption was calculated by adding these contributions in quadrature. These errors contribute minimally until the cross sections decrease rapidly at the two extremes of our measurements. At the atmospherically important wavelengths near 300 nm, the measured absorbance is uncertain to ±1.5%, except for DEK at 296 K.

3.2. Comparison to Prior Measurements

Figure 4 compares the room temperature UV absorption spectrum of MEK, DEK, and PEK determined in this work with those from previous work, as well as with that of acetone. For MEK, the International Union of Pure and Applied Chemistry (IUPAC) recommends the use of cross section measurements of Martinez et al. (1992) and IUPAC (2005). Overall, the cross sections measured in this study are in excellent agreement with the previous data from 210 to 335 nm, within 2%, 2%, and 5% of the Martinez et al. (1992) and Horowitz (1999) measurements, respectively, for MEK and DEK, and PEK.

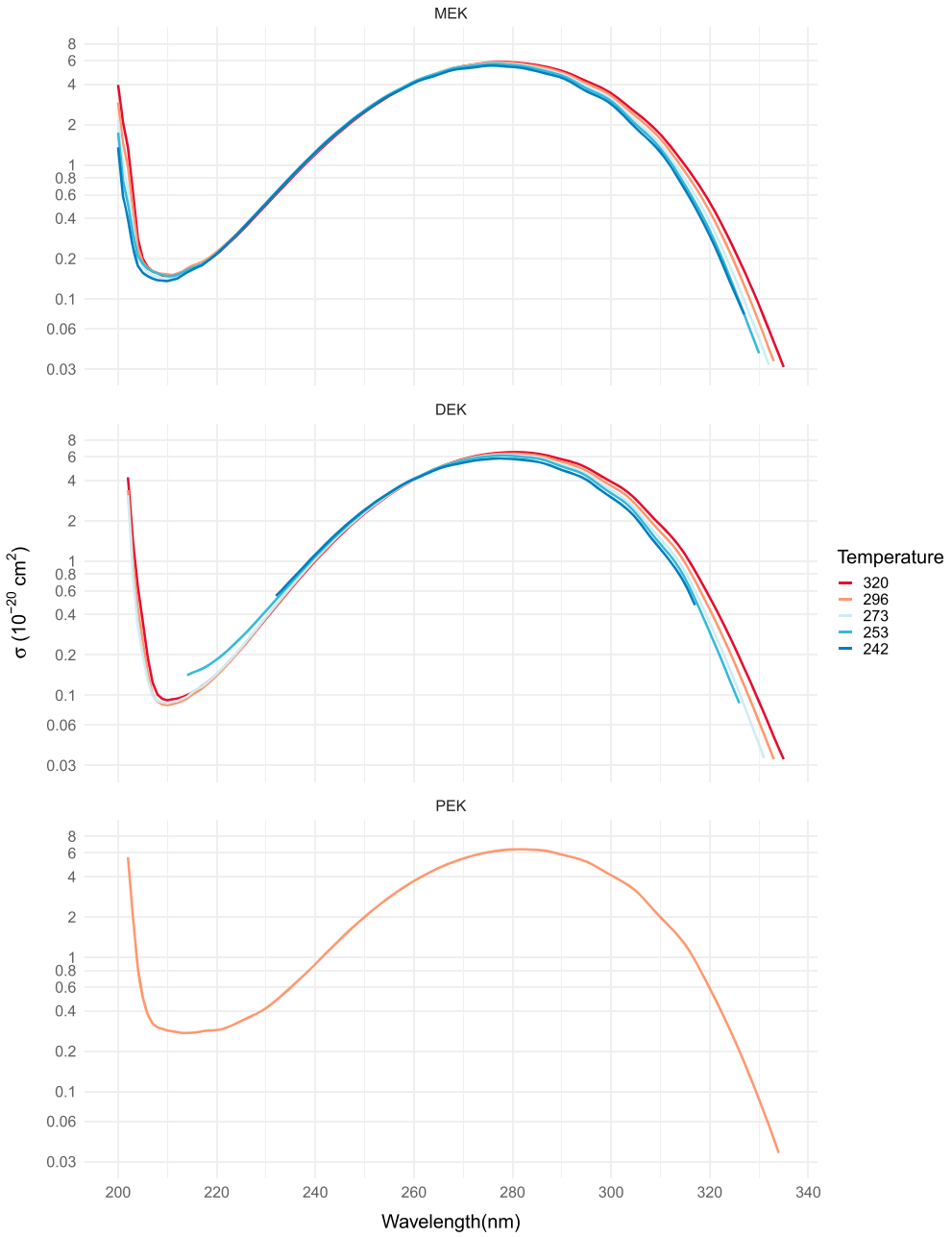

Figure 2. These panels present ultraviolet absorption cross sections (σ) in 10^{-20} cm^2 of the three species studied in this work from 200 to 340 nm. MEK ($C_2H_5C(O)CH_3$) and DEK (C_2H_5 C(O) C_2H_5) cross sections at 242, 253, 273, 296, and 320 K are shown the top two panels. DEK cross sections are shorter at 242 and 253 K due to the higher uncertainty at those lower temperatures. The third panel shows the PEK (C_2H_5 C(O) C_3H_7) cross sections at 296 K, the only temperature at which it was measured. DEK = diethyl ketone; MEK = methyl ethyl ketone; PEK = propyl ethyl ketone.

3.3. Temperature Dependencies of Cross Sections

In order to use our measured cross sections for interpolation between measured temperatures and for extrapolation beyond the temperatures our measurements, we have created a two-state model to represent the temperature dependence of the absorption cross section of C_3–C_6 saturated ketones. Following the method of Nicovich and Wine (1988) for H_2O_2 cross sections, we assume that the temperature dependence observed in the absorption cross sections of ketones arises from the changes in the population of the C = O stretch in the ground state. This methodology has already been used for acetone by Hynes et al. (1992), who also used

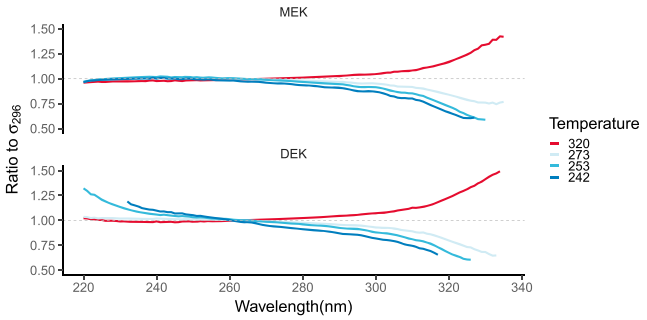

Figure 3. These panels show the ratio of absorption cross sections (σ) of MEK and DEK at various temperatures to those measured at 298 K, as a function of wavelength. DEK = diethyl ketone; MEK = methyl ethyl ketone.

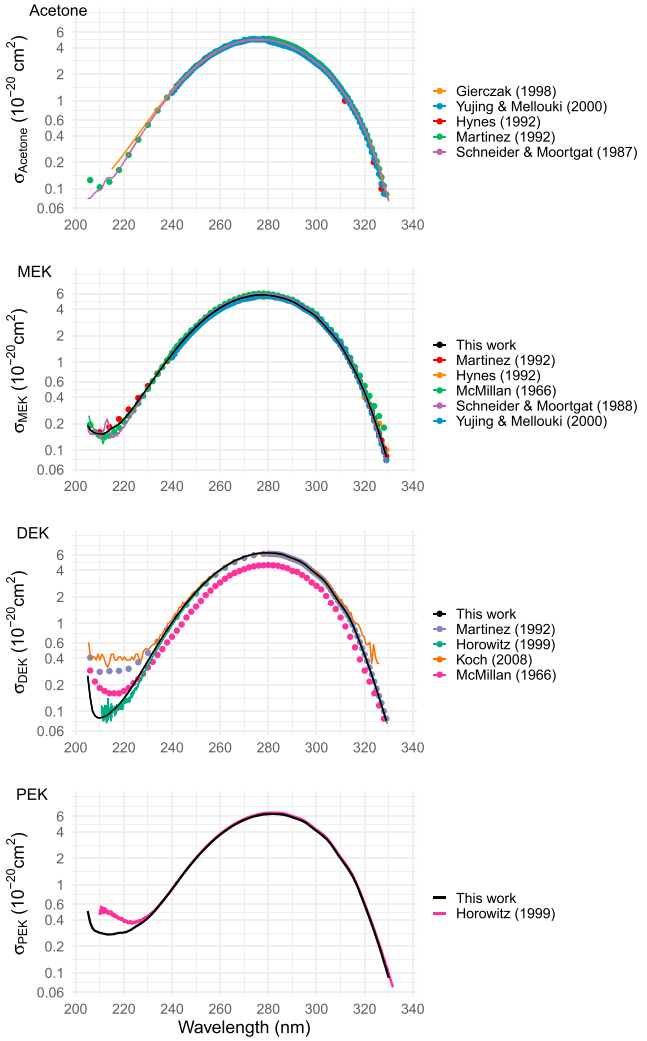

Figure 4. A comparison of the ultraviolet absorption spectra in 10^{-20} cm^2 from this (black) work with those previously reported for temperature between 294 and 300 K by various authors as compiled by the Mainz absorption cross section database (Keller-Rudek et al., 2013). DEK = diethyl ketone; MEK = methyl ethyl ketone; PEK = propyl ethyl ketone.

the model to extrapolate MEK (using only room temperature measurements) to other temperatures, using the dependence seen for acetone. The electronic transition in the carbonyl group is responsible for the UV absorption, and so we parameterize our two-state model using a carbonyl stretching frequency (ΔE) of the ketones. The carbonyl ΔE for aliphatic ketones is between 1,705 and 1,725 cm^{-1} (Silverstein et al., 1981); consequently, we expect that, at temperatures <350 K, only the first vibrationally excited state in the C = O stretch to have significant population relative to that of the ground state, and thus a model with only two states is adequate.

We model $\sigma(\lambda, T)$ of each ketone as a linear combination of $\sigma_0(\lambda)$, representing the absorption cross section for electronic excitation from ground state, and $\sigma_1(\lambda)$, representing the cross sections for electronic excitation from the first vibrational state (Nicovich & Wine, 1988). The populations in these two states are partitioned according to the fractional populations, X_0 and X_1, which are themselves functions of T and ΔE, as shown below.

$$Q = 1 + e^{\frac{-\Delta E}{RT}} \tag{2}$$

$$X_0 = \frac{1}{Q} \tag{3}$$

$$X_1 = 1 - X_0 = \frac{Q-1}{Q} \tag{4}$$

such that the overall absorption cross section is

$$\sigma(\lambda, T) = X_0(T)\sigma_0(\lambda) + X_1(T)\sigma_1(\lambda) \tag{5}$$

We fit the measured cross sections at each temperature to equation (5) while affixing ΔE at the value expected for the C = O stretch in each of the ketones. These $\sigma_0(\lambda)$ and $\sigma_1(\lambda)$ are shown below in the left column of Figure 5 for the four ketones. The second column displays model performance for each ketone compared either to our measurements (in the case of MEK and DEK) or to IUPAC recommended values (in the case of acetone). Comparable plots for PEK are displayed, but the compound is treated differently due to the lack of low-temperature data; this is discussed below. The calculated values for $\sigma_1(\lambda)$ for acetone, MEK, and DEK are realistic and comparable to those for highly absorbing species such as O_3 and NO_3 (Sander et al., 2011). We do not claim that $\sigma_0(\lambda)$ and $\sigma_1(\lambda)$ represent the cross sections from ground and excited states respectively, but they are consistent with a situation in which temperature changes impact the populations of ketone molecules in the vibrational levels of the ground state, thereby facilitating the transition of those molecules to their excited state. Additionally, although this model tends to result in specific structure in the $\sigma_1(\lambda)$ cross section and diffuse structure in the $\sigma_0(\lambda)$, we have no data to suggest that this observation is an accurate physical representation of the two states. It would be interesting to measure the cross sections at lower temperatures and at much higher temperatures. However, our model successfully represents the measured cross sections at all temperatures and wavelengths of this study. Furthermore, in the absence of experimental data, this model provides an empirical method to calculate ketone cross sections at atmospherically relevant temperatures beyond those measured in our study.

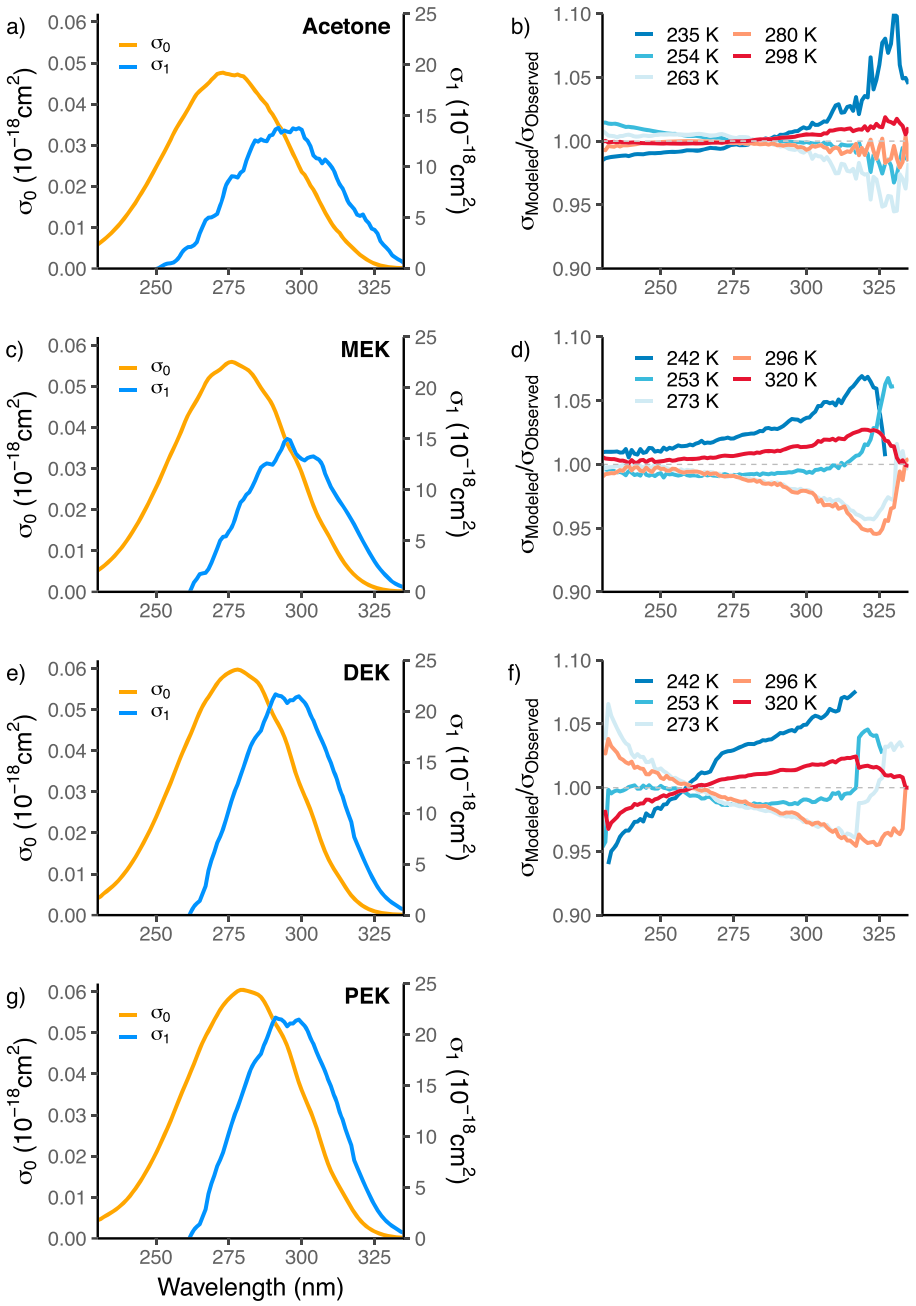

Figure 5. A two-state model for C_3–C_6 saturated ketones, parameterized with a C = O stretch frequency of 1,720 cm^{-1}. In all cases, the left column presents $\sigma_0(\lambda)$ and $\sigma_1(\lambda)$ in units of 10^{-18} cm^{-2}. $\sigma_0(\lambda)$, displayed in orange with its values on the left *y* axis, is 2–3 orders of magnitude lower than $\sigma_1(\lambda)$, displayed in blue on the right *y* axis. The right column shows the ratio of modeled σ to that observed at temperatures and wavelengths of our study. (a and b) The model results for acetone, using data from Gierczak et al. (1998). All other panels use data taken in this study. (c and d) The results for MEK. (e and f) The results for DEK. (g) The model results for PEK. DEK = diethyl ketone; MEK = methyl ethyl ketone; PEK = propyl ethyl ketone.

Using our measured data and assuming ΔE = 1,720 cm^{-1}, equation (5) gives an overdetermined system of five equations and two unknowns and can thus be solved at each nanometer increment using a QR decomposition algorithm (Gander, 1980). This solution is shown in Figure 5 below. According to this solution, $\sigma_1(\lambda)$ is ~2–3 orders of magnitude higher than $\sigma_0(\lambda)$. The performance of this model relative to observations is shown in Figure 5b as a ratio between modeled and observed $\sigma(\lambda, T)$. This model deviates only ~5% at

longer and more atmospherically relevant wavelengths, which compares well with more traditional higher order polynomials. The observed red shifting of σ_1 relative to σ_0 is also consistent with excitation from an upper vibrational state to the same electronic upper state.

In order to verify that our method works generally for short aliphatic ketones, we performed the same calculations for acetone using $\Delta E = 1{,}720\ \text{cm}^{-1}$, and the acetone spectra measured at temperatures from 235 to 298 K by Gierczak et al. (1998). In that paper, the authors improved upon the resolution of the acetone measurements relative to Hynes et al. (1992) but found that the two-state system did not reproduce their results well. However, by using $\Delta E = 1{,}720\ \text{cm}^{-1}$ and our QR decomposition methodology, we were able to produce a useful fit, comparable to the quality of fit for MEK and DEK, which is presented in Figures 5a and 5b. The $\sigma_0(\lambda)$ and $\sigma_1(\lambda)$ values in Figure 5a are comparable to those found in Figures 5c and 5e, and the fit as shown in Figure 5b is also within 5% except at the very low cross section values beyond 325 nm. The parameterized model values for $\sigma_0(\lambda)$ and $\sigma_1(\lambda)$ for all four compounds are tabulated in the supporting information (Table S2).

Because we did not measure PEK spectra at temperatures beyond room temperature, we cannot explicitly model PEK in the same way as acetone, MEK, and DEK. However, in the absence of experimental data at temperatures other than 296 K, we can use this physical model to give us an empirical basis for PEK temperature-dependent absorption; of course, this is not verified by observations and could be uncertain. If we assume that any differences between DEK and PEK spectra are due solely to differences in the ground state absorption (σ_0), it is possible to construct a usable model for the temperature dependence of the PEK spectra. As with DEK, we build the model using $\Delta E = 1{,}720\ \text{cm}^{-1}$ but affix $\sigma_0(\lambda)$ such that the model correctly represents our room temperature measurements of the PEK spectrum. Figure 5g thus closely resembles Figure 5e, with a slightly higher peak value of $\sigma_1(\lambda)$.

We considered the possibility of deriving ΔE via optimization of $\sigma_0(\lambda)$ and $\sigma_1(\lambda)$, rather than using canonical values of the C = O stretch frequency, as Hynes et al. (1992) did for acetone. We tested a range of ΔE values between 1 and 2,000 cm^{-1}. The results of this analysis are included in the supporting information (Figure S2). For MEK, aggregated error and the number of negative values is minimized at $\Delta E = 800\ \text{cm}^{-1}$ and $\Delta E = 600\ \text{cm}^{-1}$, respectively, which is similar to $\Delta E = 950\ \text{cm}^{-1}$ found by Hynes et al. (1992) for acetone. At 350 K, $\Delta E = 600\ \text{cm}^{-1}$ implies that 7.8% of molecules would be in the first vibrationally excited level, which may challenge our assumption of a two-state model (i.e., the population in the next vibrational level would not be negligible). The larger value of ΔE ensures that a two-state model is reasonable over the temperature range of our study.

Regardless of which ΔE is used, this two-state model allows us to extrapolate our data to temperatures outside of the range we were able to measure. Neither choice of ΔE causes large discontinuities in σ relative to measured values when modeled at temperatures up to 350 and down to 160 K. As one might expect from comparing the relative magnitudes of $\sigma_0(\lambda)$ and $\sigma_1(\lambda)$ in Figures 5a, 5c, and 5e, the model parameterized with $\Delta E = 1{,}720\ \text{cm}^{-1}$ produces a smaller temperature response with decreasing temperatures relative to the model parameterized with $\Delta E = 600$, while the reverse is true at temperatures >350 K. Whichever parameterization is chosen, the model produces usable results at atmospherically relevant temperatures outside the range of measurements. Figure S3 shows the performance of the model at these extreme values. For atmospheric applications, we provide models parameterized at $\Delta E = 1{,}720\ \text{cm}^{-1}$, whose $\sigma_0(\lambda)$ and $\sigma_1(\lambda)$ values are provided in the supporting information (Table S2). We also include an R program (Brewer_JValue_Subroutines_Code_S1.R) that can use the two-state models provided in Table S2 to output cross sections at any atmospherically relevant temperature. This code will be discussed in more detail below.

As many modeling applications of J value calculation take place in demanding computation environments (e.g., in the context of a globally resolved chemical transport model), modeling applications of cross sections tend to use some form of wide-band average binning in order to efficiently and accurately compute J values, such as the Fast-J (Wild et al., 2000) binning schemes. As such, we believe that adapting our data for a wide array of binning schemes will be most useful in facilitating its future use by the community. Thus, we have produced a Fast-J (Wild et al., 2000) treatment of our cross section data, which is included in the supplement to this paper (Table S4). In the code supplement to this paper, we have also included an R program capable of binning our data in other binning schemes; this code is also discussed further in section 3.5.

3.4. Calculated J Value Comparisons

The first-order rate coefficient for the removal of ketones, the J value (s^{-1}), is given by equation (6):

$$J = \int_{\lambda_1}^{\lambda_2} \sigma(\lambda, T) \times \Phi(\lambda, T, P) \times F(\theta, \lambda) \quad (6)$$

where F is the actinic flux (quanta·cm^{-2}·s^{-1}·nm^{-1}), Φ is the quantum yield for the destruction of the molecule, $\sigma(\lambda, T)$ is the absorption cross section (cm^2) of the molecule, and λ_1 and λ_2 are the limits of wavelengths available in the atmosphere over which the molecule absorbs,

We have calculated J values for each compound using model-derived clear-sky actinic flux to roughly show the photolytic loss rate coefficients for these ketones in the troposphere. We used the National Center for Atmospheric Research tropospheric ultraviolet visible (TUV) radiative transfer model version 5.3.1 (publicly available at https://www2.acom.ucar.edu/modeling/tropospheric-ultraviolet-and-visible-tuv-radiation-model) to simulate monthly average solar noon actinic flux in 10° latitude bins for a variety of altitudes. This model uses the top of atmosphere irradiance modified by scattering and absorption to calculate an actinic flux for a given condition using a four-stream pseudospherical approximation (Madronich & Flocke, 1999).

Figure 6 shows the calculated J values for MEK for quantum yields from IUPAC recommendations and Romero et al. (2005). For each of these quantum yields, we calculate J values using two sets of cross sections: (1) modeled temperature-dependent cross sections as per section 3.3 of this paper and (2) the IUPAC recommended room temperature cross sections from Martinez et al. (1992), referred to as $\sigma_{Martinez}$ in Figure 6. Quantum yields and cross sections were calculated using the same reanalysis-derived temperature and pressure data in order to ensure that both factors vary simultaneously, as they do in the real atmosphere. Additionally, we compare these photolysis rate coefficients to the rate coefficients for removal of MEK by reaction with OH. Concentrations of OH were from Spivakovsky et al. (2000) that does not include any HO_x produced from the oxidation of MEK, DEK, or PEK. The rate coefficients for OH reaction with the various ketones are taken from Calvert et al. (2011). The temperature, pressure, and OH profiles used to generate this plot are included in the supporting information (Table S3), as are the R programs used to calculate all the quantum yields used in this paper (Brewer_JValue_Subroutines_Code_S1.R), discussed in section 3.5 below.

Figure 6 shows that, for all three compounds, the inclusion of the temperature-dependent cross sections leads to a decrease in the J value in the upper troposphere. In these specific location, season, and cloudless conditions, the change is on the order of 20–25%. Figure S4 in the supporting information replicates Figure 6 with an assumed cloud optical depth of 25% and 100% cloud cover; the change in the J value due to the temperature dependence is unaffected by this parameter and remains on the order of 20–25%. Because the reference IUPAC values are for 296 K, we expect a decrease in the J value as a result of using our temperature-dependent cross sections, which decrease with temperature. In addition, Figure 6a shows that the choice of quantum yield is important to understanding the change of J value with altitude, especially under upper tropospheric conditions. Irrespective of cross section used, the inclusion of the wavelength-dependent QY from Romero et al. (2005) decreases the J value relative to the IUPAC QY recommendation below 6 km; above 6 km, using these cross sections increases the J value relative to the IUPAC recommendations. Furthermore, because no experimental studies of PEK quantum yields are known, Figures 6e and 6f assume a quantum yield of 1 at all wavelengths and pressures, which accounts for the different shapes of the vertical J value profile in Figure 6e as compared to Figures 6a and 6c; the calculated J values are, therefore, upper bounds for PEK loss. These observations point to a need for more detailed quantum yield measurements for these species as well. Finally, Figure 6 shows that loss rates to photolysis are larger than due to reaction with OH at all altitudes for MEK and above 5 km for DEK and PEK.

Figure 7 presents MEK J values in the troposphere derived using our measured temperature-dependent cross sections at local solar noon at each 10° latitude bin (i.e., −90, −80, ... , 80, 90) during four different months representative of seasons: January (boreal winter), April (boreal spring), July (boreal summer), and October (boreal autumn). This is done to exemplify how photolysis rate coefficient changes with location and season. Photolysis rate coefficients are largest in the tropical tropopause throughout the year, with J values reaching ~2×10^5 s^{-1}. However, this figure uses actinic flux characteristic of a cloudless sky and constant aerosol

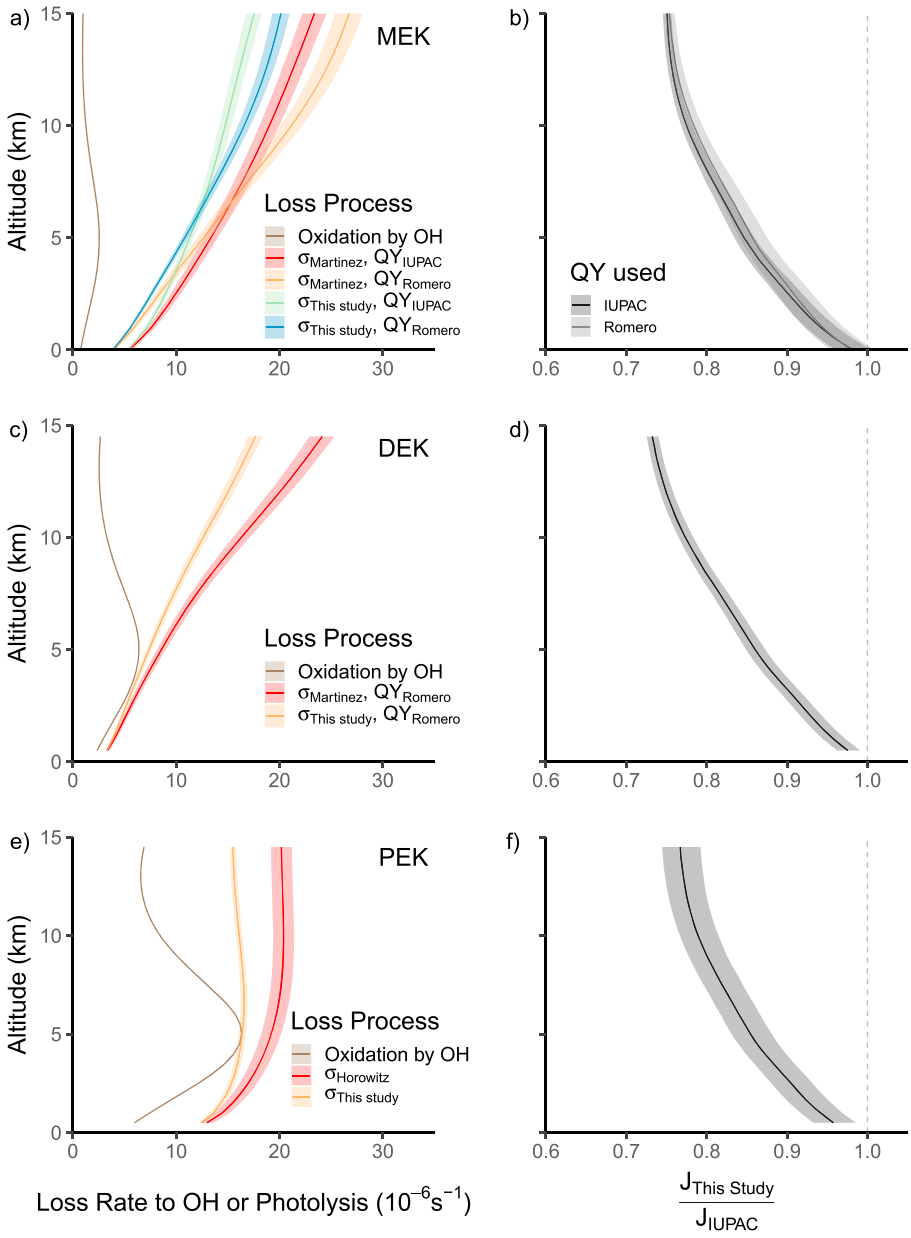

Figure 6. (a) Photolytic and OH-reaction loss rate coefficients (10^{-6} s^{-1}) for MEK in April at the equator with no clouds present. J values are calculated using two different absorption cross sections (from this study and Martinez et al., 1992) and two different quantum yield possibilities. Shaded areas in plots (a), (c), and (e) represent the upper and lower bounds of uncertainty in the cross sections propagated through to the J value. The quantum yields are from the IUPAC recommendations (International Union of Pure and Applied Chemistry, 2005) and Romero et al. (2005). (b) The ratio of the J values calculated with our cross sections to those using the IUPAC recommendations for each quantum yield used (International Union of Pure and Applied Chemistry, 2005). Shaded area in plots (b), (d), and (f) represent the ratio between the upper (and lower) bounds of this study's calculated J values to the upper (and lower) bounds of the J values calculated according IUPAC cross sections. Panels (c) and (e) show DEK and PEK J values under the same conditions. These J values are also calculated using two different absorption cross sections but using only the quantum yield from Romero et al. (2005) for DEK and an assumed quantum yield of 1 for PEK. J value uncertainties in (a), (c), and (e) reflect only the uncertainties in cross sections and not those in the various quantum yields used. Panels (d) and (f) show the same ratio as panel (b), calculated for DEK and PEK, which each use only one quantum yield. DEK = diethyl ketone; MEK = methyl ethyl ketone; PEK = propyl ethyl ketone; IUPAC = International Union of Pure and Applied Chemistry.

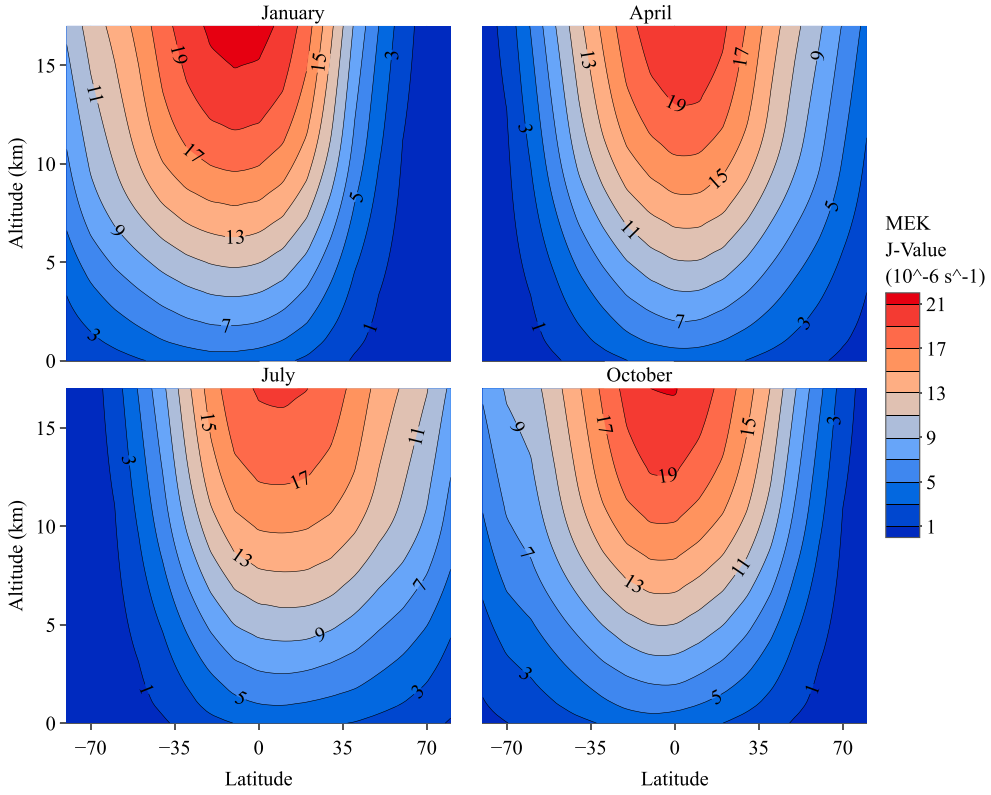

Figure 7. The contours here show methyl ethyl ketone (MEK) J values in 10^{-6} s^{-1} for four seasons. Pressures and temperatures used to generate these values are 10-year (2007–2017) monthly means from National Centers for Environmental Prediction reanalysis; the cross sections used are from the two-state model presented in this study; the quantum yields are from Romero et al. (2005). The actinic fluxes are used in this plot are solar noon values created using a customized tropospheric ultraviolet visible model run. We used the photochemistry-optimized standard tropospheric ultraviolet visible input file with the following specific conditions: (1) We used a four year total pre-stratospheric-depletion O_3 column values (mean monthly values from 1978 to 1982) from the TOMS instrument aboard the Nimbus 7 (Keating et al., 1989); 2) We assumed clear sky, and we fixed the surface albedo value at 0.1 irrespective of surface type (i.e., water or land); (3) We used an aerosol single scattering albedo of 0.99; we used a continental aerosol profile (aerosol optical depth at 550 nm = 0.235; Elterman, 1968); and (5) We used temperature and pressure profiles from a 2007–2017 average of monthly National Center for Atmospheric Research National Centers for Environmental Prediction reanalysis data (Kalnay et al., 1996). These assumptions were chosen to create a simplified model output that others could easily replicate.

optical depth, as such it should be primarily be treated as a comparison with modeled photolysis rates coefficients and quick look up. It is not meant to represent true atmospheric values. A similar pattern and rough values are to be expected for DEK or PEK. These rates will change depending upon the parameters specific to various atmospheric models; however, we include this generalized example for illustrative purposes. As to be expected, the photolysis maximizes in the tropical upper troposphere. From Figure 6, it appears that for MEK, photolysis is likely to be more important than loss to OH, regardless of the quantum yield used. For PEK and DEK, the two loss processes compete in the lower troposphere. Our study highlights the need for elucidation of the quantum yields of these species under atmospheric conditions.

MEK is an understudied but relatively abundant ketone in the troposphere, with abundances up to 25% of that of acetone (Yañez-Serrano et al., 2016). Its inclusion and accurate representation in global chemical transport models is potentially an important part of making those models fully represent the tropospheric HO_x budget, especially in the upper troposphere. Our work suggests that the inclusion of the temperature dependence we measured is useful to correctly representing MEK chemistry in the troposphere. DEK and PEK atmospheric abundances are unknown, but the similar photolytic properties of these compounds suggest that, if found in abundance, they could also impact global oxidative potential.

3.5. Implementation in R

The schemes presented here have been implemented as a program in R, an open-source programming environment (R Development Core Team, 2010), which is available on all operating systems. The program (Brewer_JValue_Subroutines_Code_S1.R) makes use of multiple nested subroutines and wrapper functions in order to perform three computations:

1. Use the two-state models provided in Table S2 to output a cross section for MEK, DEK, PEK, or acetone at any atmospherically relevant temperature.
2. Calculate the quantum yields for MEK, DEK, or PEK used in Figure 6.
3. Bin any quantum yield, cross section, or actinic flux according to a given wide-band binning scheme, such as those found in global models or other applications where calculation speed must be given highest priority (Wild et al., 2000).

The modular approach to the code included allows additional quantum yield schemes to be added in as separate functions, which can be called in their own right. Moreover, the code to perform the wide-band binning is extensible and should be usable for most binning schemes; the details are discussed further in the supporting information. Finally, this paper also includes an additional program (Brewer_JValue_Example_Code_S2.R), which gives an example implementation of the subroutines included in Brewer_JValue_Subroutines_Code_S1.R.

4. Summary

1. We present new measurements of MEK and DEK absorption cross sections at temperatures between 242 and 320 K and of PEK at 298 K between 200 and 335 nm. We use these measured values to refine our understanding of the role of photolysis in the tropospheric chemistry of these compounds.
2. We show that the measured cross sections are robustly represented by a two-state model. While we do not have data to assess the accuracy of the model at temperatures below 242 K, this model can be extrapolated to temperatures below our measurements to provide empirical, numerically stable, and physically reasonable ketone cross sections at all tropospherically relevant temperatures. We further show that this same model also allows us to simulate the temperature dependence of acetone UV absorption cross sections and we suggest that an analogous treatment works for PEK.
3. For MEK, DEK, and PEK, the inclusion of temperature dependence leads to a decrease in photolysis rate coefficients of up to 20–25%, when compared to photolysis rate coefficients derived using available room temperature literature recommendations. This decrease is largest in the upper troposphere (Figures 6 and 7), where ketone photolysis is thought to be most important to global oxidation potential.
4. We provide a set of calculated J values for easy comparison at both 1 nm and wide-binned resolutions and produce first-order estimates of photolysis rates in the troposphere. We also provide the code necessary to extend and modify this work as needed in future applications.

Acknowledgments
This work was funded by NASA Award NNX16AI17G and by the European Union's Horizon 2020 research and innovation program through the EUROCHAMP-2020 Infrastructure Activity under grant agreement 730997. This work was funded in part by NOAA's climate and health of the atmosphere research programs. All data from this paper are included in the supporting information.

References

Brewer, J. F., Bishop, M., Kelp, M., Keller, C., Ravishankara, A. R., & Fischer, E. V. (2017). A sensitivity analysis of key factors in the modeled global acetone budget. *Journal of Geophysical Research: Atmospheres*, *122*, 2043–2058. https://doi.org/10.1002/2016JD025935

Calvert, J. G., Mellouki, A., Orlando, J. J., Pilling, M. J., & Wallington, T. J. (2011). *The Mechanisms of Atmospheric Oxidation of the Oxygenates*. New York: Oxford University Press.

Collerson, R. R., Counsell, J. F., Handley, R., Martin, J. F., & Sprake, C. H. (1965). Purification and vapour pressures of some ketones and ethers. *Journal of the Chemical Society*, (0), 3697–3700. http://pubs.rsc.org/en/content/articlepdf/1965/jr/jr9650003697, https://doi.org/10.1039/jr9650003697

Elterman, L. (1968). UV, visible, and IR attenuation for altitudes to 50 km (AFCRL-68-0153). Retrieved from Cambridge, Mass.:

Gander, W. (1980). Algorithms for the QR-decomposition. Retrieved from Zurich, CH:

Gierczak, T., Burkholder, J. B., Bauerle, S., & Ravishankara, A. R. (1998). Photochemistry of acetone under tropospheric conditions. *Chemical Physics*, *231*(2-3), 229–244. https://doi.org/10.1016/S0301-0104(98)00006-8

Grant, D. D., Fuentes, J. D., Chan, S., Stockwell, W. R., Wang, D., & Ndiaye, S. A. (2008). Volatile organic compounds at a rural site in western Senegal. *Journal of Atmospheric Chemistry*, *60*(1), 19–35. https://doi.org/10.1007/s10874-008-9106-1

Haas, Y. (2003). Photochemical a-cleavage of ketones: Revisiting acetone. *Photochemical and Photobiological Sciences*, *3*, 6–16.

Horowitz, A. (1999). *Absorption cross sections of 2-pentanone, 3-pentanone, and 3-hexanone*. Mainz, Germany. Retrieved from: The Max-Planck-Institut für Chemie. http://satellite.mpic.de/spectral_atlas/cross_sections/Organics%20(carbonyls)/Ketones,ketenes/C2H5C(O)C3H7_Horowitz(1999)_298K_209-369nm.txt

Hynes, A. J., Kenyon, E. A., Pounds, A. J., & Wine, P. H. (1992). Temperature dependent absorption cross-sections for acetone and n-butanone—Implications for atmospheric lifetimes. *Spectrochimica Acta*, *48A*(9), 1235–1242.

International Union of Pure and Applied Chemistry (IUPAC) (2005). IUPAC Task Group on Atmospheric Chemical Kinetic Data Evaluation—Data Sheet P8. In CH3C(O)C2H5.

Kalnay, E., Kanamitsu, M., Kistler, R., Collins, W. J., Deaven, D., Gandin, L., et al. (1996). The NCEP/NCAR 40-year reanalysis project. *Bulletin of the American Meteorological Society*, *77*(3), 437–471. https://doi.org/10.1175/1520-0477(1996)077%3C0437:TNYRP%3E2.0.CO;2

Keating, G. M., Pitts, M. C., & Young, D. F. (1989). Ozone reference models for the middle atmosphere. In G. M. Keating (Ed.), *Middle Atmosphere Program Handbook for MAP* (Vol. 31, pp. 37–49). Urbana: SCOSTEP Secretariat, University of Illinois.

Keller-Rudek, H., Moortgat, G. K., Sander, R., & Sörensen, R. (2013). The MPI-Mainz UV/VIS spectral atlas of gaseous molecules of atmospheric interest. *Earth System Science Data*, *5*(2), 365–373. https://doi.org/10.5194/essd-5-365-2013

Koch, J. D., Gronki, J., & Hanson, R. K. (2008). Measurements of near-UV absorption spectra of acetone and 3-pentanone at high temperatures. *Journal of Quantitative Spectroscopy & Radiative Transfer*, *109*(11), 2037–2044. https://doi.org/10.1016/j.jqsrt.2008.02.010

Koch, J. D., & Hanson, R. K. (2003). Temperature and excitation wavelength dependencies of 3-pentanone absorption and fluorescence for PLIF applications. *Applied Physics B: Lasers and Optics*, *76*(3), 319–324. https://doi.org/10.1007/s00340-002-1084-4

Madronich, S., & Flocke, F. (1999). The role of solar radiation in atmospheric chemistry. In P. Boule (Ed.), *Environmental Photochemistry* (pp. 1–26). Berlin, Heidelberg: Springer Berlin Heidelberg. https://doi.org/10.1007/978-3-540-69044-3_1

Majer, V., Svoboda, V., & Kehiaian, H. V. (1985). *Enthalpies of vaporization of organic compounds: A critical review and data compilation*. Oxford: Blackwell Scientific Oxford.

Martinez, R. D., Buitrago, A. A., Howell, N. W., Hearn, C. H., & Joens, J. A. (1992). The near U.V. absorption spectra of several aliphatic aldehydes and ketones at 300 K. *Atmospheric Environment*, *26A*(5), 785–792.

McKeen, S. A., Gierczak, T., Burkholder, J. B., Wennberg, P. O., Hanisco, T. F., Keim, E. R., et al. (1997). The photochemistry of acetone in the upper troposphere: A source of odd-hydrogen radicals. *Geophysical Research Letters*, *24*(24), 3177–3180. https://doi.org/10.1029/97GL03349

McMillan, V. (1966). *Absorption cross-sections of various organic compounds. Photochemistry*. New York: John Wiley & Sons.

Moore, D. P., Remedios, J. J., & Waterfall, A. M. (2012). Global distributions of acetone in the upper troposphere from MIPAS spectra. *Atmospheric Chemistry and Physics*, *12*(2), 757–768. https://doi.org/10.5194/acp-12-757-2012

Nádasdi, R., Kovács, G., Szilágyi, I., Demeter, A., Dóbé, S., Bérces, T., & Márta, F. (2007). Exciplex laser photolysis study of acetone with relevance to tropospheric chemistry. *Chemical Physics Letters*, *440*(1-3), 31–35. https://doi.org/10.1016/j.cplett.2007.04.014

Neumaier, M., Ruhnke, R., Kirner, O., Ziereis, H., Stratmann, G., Brenninkmeijer, C. A. M., & Zahn, A. (2014). Impact of acetone (photo) oxidation on HOx production in the UT/LMS based on CARIBIC passenger aircraft observations and EMAC simulations. *Geophysical Research Letters*, *41*, 3289–3297. https://doi.org/10.1002/2014GL059480

Nicovich, J. M., & Wine, P. H. (1988). Temperature-dependent absorption cross sections for hydrogen peroxide vapor. *Journal of Geophysical Research*, *93*(D3), 2417–2421. https://doi.org/10.1029/JD093iD03p02417

Papanastasiou, D. K., Feierabend, K. J., & Burkholder, J. B. (2011). Cl2O photochemistry: Ultraviolet/vis absorption spectrum temperature dependence and O(3P) quantum yield at 193 and 248 nm. *The Journal of Chemical Physics*, *134*(20), 204310. https://www.ncbi.nlm.nih.gov/pubmed/21639443, https://doi.org/10.1063/1.3592662

R Development Core Team (2010). R: A language and environment for statistical computing. Retrieved from http://www.r-project.org

Romero, M. T. B., Blitz, M. A., Heard, D. E., Pilling, M. J., Price, B., Seakins, P. W., & Wang, L. (2005). Photolysis of methylethyl, diethyl and methylvinyl ketones and their role in the atmospheric HOx budget. *Faraday Discussions*, *130*, 73. https://doi.org/10.1039/b419160a

Sander, S. P., Abbatt, J., Barker, J. R., Burkholder, J. B., Friedl, R. R., Golden, D. M., et al. (2011). Chemical kinetics and photochemical data for use in atmospheric studies, Evaluation Number 17. Retrieved from Pasadena, CA: http://jpldataeval.jpl.nasa.gov/

Sharpe, S. W., Johnson, T. J., Sams, R. L., Chu, P. M., Rhoderick, G. C., & Johnson, P. A. (2004). Gas-phase databases for quantitative infrared spectroscopy. *Applied Spectroscopy*, *58*(12), 1452–1461. https://doi.org/10.1366/0003702042641281

Siegel, H., & Eggerdorfer, M. (1985). Ketones. In *Ullmann's encyclopedia of industrial chemistry* (Vol. A15, pp. 77–95). Weinheim, Germany: Wiley-VCH.

Silverstein, R. M., Bassler, G. C., & Morrill, T. C. (1981). *Spectrometric identification of organic compounds*. New York: John Wiley.

Singh, H. B., Kanakidou, M., Crutzen, P. J., & Jacob, D. J. (1995). High concentrations and photochemical fate of oxygenated hydrocarbons in the global troposphere. *Nature*, *378*(6552), 50–54. https://doi.org/10.1038/378050a0

Singh, H. B., Salas, L. J., Chatfield, R. B., Czech, E., Fried, A., Walega, J., et al. (2004). Analysis of the atmospheric distribution, sources, and sinks of oxygenated volatile organic chemicals based on measurements over the Pacific during TRACE-P. *Journal of Geophysical Research*, *109*, D15S07. https://doi.org/10.1029/2003JD003883

Spivakovsky, C. M., Logan, J. A., Montzka, S. A., Balkanski, Y. J., Foreman-Fowler, M., Jones, D. B. A., et al. (2000). Three-dimensional climatological distribution of tropospheric OH: Update and evaluation. *Journal of Geophysical Research*, *105*(D7), 8931–8980. https://doi.org/10.1029/1999JD901006

Wennberg, P. O., Hanisco, T. F., Jaegle, L., Jacob, D. J., Hintsa, E. J., Lanzendorf, E. J., et al. (1998). Hydrogen radicals, nitrogen radicals, and the production of O_3 in the upper troposphere. *Science*, *279*(5347), 49–53. https://doi.org/10.1126/science.279.5347.49

Wild, O., Zhu, X., & Prather, M. J. (2000). Fast-J: Accurate simulaton of in- and below-cloud photolysis in tropospheric chemical models. *Journal of Atmospheric Chemistry*, *37*(3), 245–282. https://doi.org/10.1023/A:1006415919030

Yañez-Serrano, A. M., Nolscher, A. C., Bourtsoukidis, E., Derstroff, B., Zanoni, N., Gros, V., et al. (2016). Atmospheric mixing ratios of methyl ethyl ketone (2-butanone) in tropical, boreal, temperate, and marine environments. *Atmospheric Chemistry and Physics*, *16*(17), 10,965–10,984. https://doi.org/10.5194/acp-16-10965-2016

Yujing, M., & Mellouki, A. (2000). The near-UV absorption cross sections for several ketones. *Journal of Photochemistry and Photobiology*, *134*(1-2), 31–36. https://doi.org/10.1016/S1010-6030(00)00243-4